



MRI of Pediatric Orbital Masses: Role of Quantitative Diffusion-weighted Imaging in Differentiating Benign from Malignant Lesions

Alok Jaju¹ · Karen Rychlik² · Maura E. Ryan¹

Received: 16 July 2018 / Accepted: 30 April 2019 / Published online: 27 May 2019
© Springer-Verlag GmbH Germany, part of Springer Nature 2019

Abstract

Purpose To systematically evaluate the utility of different magnetic resonance imaging (MRI) features, including quantitative diffusion-weighted imaging, in differentiating benign from malignant pediatric orbital masses.

Methods The use of MRI in 40 pediatric patients with orbital masses was retrospectively reviewed. Multiple subjective and objective MRI parameters, including lesion mean apparent diffusion coefficient (ADC) values and lesion-to-thalamus ADC ratio were recorded. Bivariate analysis was done to identify parameters that were significantly different between benign and malignant subgroups. Receiver operating curves were used to establish optimal cut-off values for lesion mean ADC and lesion-to-thalamus ADC ratio for predicting benign versus malignant lesions.

Results Lesion mean ADC, lesion-to-thalamus ADC ratio and extent of contrast enhancement showed statistically significant differences between the two subgroups. For distinguishing benign from malignant lesions, a lesion mean ADC cut-off value of 1.14×10^{-3} mm²/s provided a sensitivity of 84% and specificity of 100%, while an ADC ratio of 1.4 provided a sensitivity of 81% and specificity of 89%.

Conclusion Quantitative diffusion-weighted imaging can be a useful adjunct in characterizing pediatric orbital masses by MRI, and thus help in clinical decision making.

Keywords Pediatric · Orbital masses · MRI · DWI · ADC

Introduction

Pediatric orbital masses are relatively uncommon but include a wide range of benign and malignant entities [1]. Although clinical symptoms and signs can help differentiate these to some extent, often they are not specific enough. Distinguishing benign from malignant lesions is of paramount importance because of vastly different treatment approaches and prognosis. A malignant tumor, if not treated promptly, can rapidly threaten sight and life, while a benign tumor may require nothing more than observation. The or-

bit is also a difficult site to biopsy, with limited accessibility and high risk of complications. Imaging plays a key role in identification, defining the extent and characterization of these lesions.

Magnetic resonance imaging (MRI) is the mainstay for imaging most orbital masses, although computed tomography (CT) and ultrasound can have ancillary roles; however, on routine MRI sequences, there can be significant overlap of findings between benign and malignant lesions [2–5]. Diffusion-weighted imaging (DWI) has been used for differentiating between benign and malignant tumors in various body parts. There is some existing literature on DWI in orbital tumors, although most studies have been performed on adult or combined adult and pediatric populations [6–9]; however, the histological spectrum of orbital tumors and resulting diagnostic conundrums in children are very different from adults and should be considered separately.

This study aimed to evaluate MRI features of pediatric orbital masses with emphasis on quantitative DWI.

✉ Alok Jaju
ajaju@luriechildrens.org

¹ Department of Medical Imaging, Ann & Robert H. Lurie Children's Hospital of Chicago, Northwestern University Feinberg School of Medicine, 225 E. Chicago Ave, Chicago, IL 60611, USA

² Stanley Manne Children's Research Institute, Ann and Robert H. Lurie Children's Hospital of Chicago, Department of Pediatrics, Northwestern University Feinberg School of Medicine, 225 E. Chicago Ave, Chicago, IL 60611, USA

Methods

Data Collection

This was a retrospective study conducted at a large free-standing Children's Hospital. The study was approved by the Institutional Review Board with waiver for informed consent, and compliant with Health Insurance Portability and Accountability Act (HIPAA). A database search of the picture archiving and communications system (PACS) was done to identify patients with orbital masses who presented from 2005 to 2014.

Inclusion criteria were age under 18 years, diagnosis of soft tissue extraocular orbital mass by MRI, and availability of MRI with DWI, prior to surgery, biopsy or treatment. The MRI studies done at outside institutions but uploaded in the institutional PACS were also included. Lesions less than 5 mm in the long axis were excluded because of difficulty in obtaining an accurate apparent diffusion coefficient (ADC) measurement. Patients with history of neurofibromatosis-1 (NF1) and optic pathway lesions compatible with low grade glioma were excluded, as this is a straightforward diagnosis that does not cause diagnostic confusion with other conditions. Also, this center sees a very large number of NF1-related optic pathway gliomas, and including these may have skewed the results. Intraocular lesions, including retinoblastomas, as well as lesions of the bony orbit were not included in the scope of the study. Electronic medical records of the patients were reviewed to collect baseline data including age, sex and presenting symptoms. A detailed review of the clinical notes, laboratory and pathology reports was performed. The lesions were classified into benign and malignant categories. For lesions that were biopsied or resected, this was based on histopathology reports, while for the lesions that did not have tissue sampling, this determination

was based on clinical and imaging follow up, and the duration of follow-up was noted.

The MRI studies were reviewed by a pediatric neuro-radiologist. The studies were performed on a variety of scanners from different vendors, including both 1.5 and 3 T field strengths, and varying technical parameters. Some patients underwent sedation or general anesthesia as per the department policy for clinical MRI studies that takes the patient's age, weight and American Society of Anesthesiologists (ASA) score into account. For the studies obtained at this institution, the diffusion-weighted images were obtained using single-shot, spin echo, echo planar technique (DW-SE-EPI) typically with the following parameters: 5 mm slice thickness with 1 mm interslice gap, repetition time 6900 msec, average echo time 93 msec, field of view 230 × 230, matrix of 192 × 192, and b-values of 0 and 1000. Also included was a lesion-to-thalamic ADC ratio as an internal control to account for potential technical variability.

The anonymized images were analyzed on a Centricity PACS viewer (General Electric, Barrington, IL, USA). The MRI lesion characteristics that were recorded included laterality, location, margins, size, subjective DWI signal, lesion mean ADC value, lesion-to-thalamus ADC ratio, subjective assessment of T2 and T1 signals, and enhancement pattern including extent and intensity of enhancement. Subjective categorization of the lesion margins was done as ill-defined versus well-defined. The lesion size was expressed as a product of three perpendicular dimensions in cm³. Comparison with normal appearing gray matter was performed to categorize the lesions as bright, dark or intermediate on the T1, T2 and DWI sequences. The lesion mean ADC value was measured by drawing the largest possible ellipsoid region of interest (ROI) through the apparently solid portion of the lesion, taking care to avoid volume av-

Table 1 Distribution of orbital lesions by pathology, and respective lesion ADC values and lesion-to-thalamus ADC ratios for each subtype

	<i>N</i>	Age (months) median (IQR)	Lesion ADC (10 ⁻³ mm ² /s) Median (IQR)	ADC ratio median (IQR)
<i>Benign</i>	31	40 (5–71)	1.5 (1.2–2)	1.8 (1.5–2.5)
Venolymphatic malformation	10	43.5 (2–68)	1.9 (1.4–2.3)	2.4 (1.8–2.7)
Hemangioma	8	7.5 (4–47.5)	1.5 (1.3–1.8)	1.8 (1.6–2.1)
Plexiform neurofibroma	2	86 (47–125)	2.3 (2.2–2.4)	2.7 (2.5–2.9)
Infection/pseudotumor	3	64 (25–189)	0.9 (0.5–1.6)	1.1 (0.7–2.1)
Hamartoma	1	7	1.6	1.9
Dacryocystocele	1	30	1.3	1.6
Unspecified benign lesions	6	75 (68–108)	0.9 (0.8–1.1)	1.2 (1.1–1.4)
<i>Malignant</i>	9	108 (74–115)	0.8 (0.7–1)	1.1 (0.9–1.3)
Rhabdomyosarcoma	6	74.5 (68–108)	0.9 (0.8–1.1)	1.2 (1.1–1.9)
Leukemia	2	183 (170–196)	0.6 (0.5–0.7)	0.8 (0.7–0.9)
Langerhans cell histiocytosis	1	113	0.8	1

IQR interquartile range, *ADC* apparent diffusion coefficient

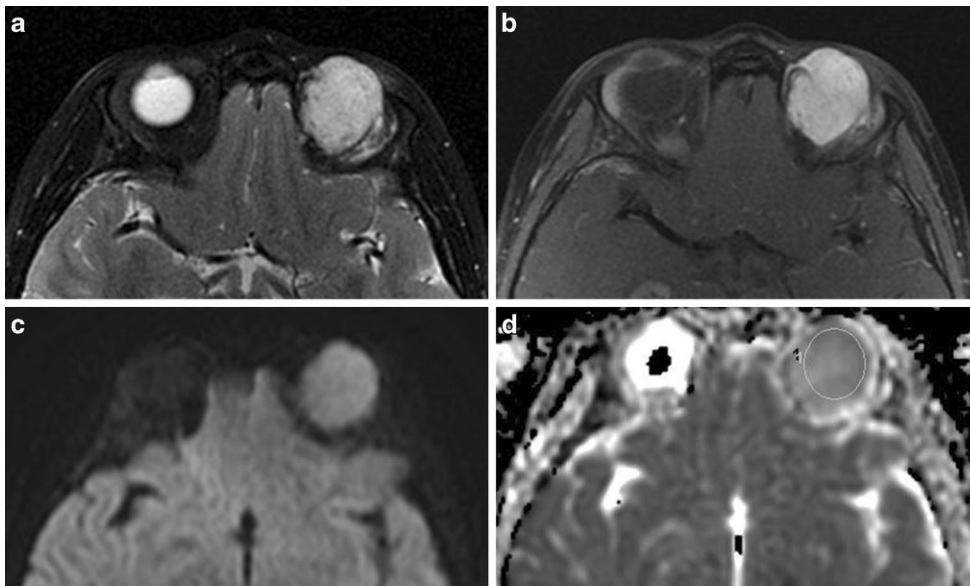


Fig. 1 A 6-year-old girl presenting with proptosis. MRI of the orbits with axial T2 fat-saturated image (a), axial post-contrast T1 fat-saturated image (b), axial diffusion-weighted image (c) and axial ADC image with ROI placement (d). There is a mass in the left orbit that is T2 hyperintense with avid, homogeneous post-contrast enhancement. On the T2 weighted and post-contrast T1 weighted sequences, the mass resembles a hemangioma/vascular lesion; however, the mass has intermediate diffusion signal, with mean ADC of $1.14 \times 10^{-3} \text{ mm}^2/\text{s}$ and ADC to thalamic ratio of 1.4. These are at the cut-off values suggested in this study and raise suspicion for a malignant lesion. The lesion rapidly grew over a 2-week follow-up (not shown), and was determined to be an embryonal rhabdomyosarcoma by histopathology

eraging with adjacent structures particularly fat and bone as well as any cystic or necrotic components of the mass. Correlation with T2 and postcontrast T1-weighted images was done to ensure accurate ROI placement. The mean ADC value of normal appearing left thalamus was obtained for each patient by drawing an ellipsoid ROI (30–80 mm²) covering at least 50% cross-sectional area of the thalamus on axial image, and the ratio of lesion mean ADC to thalamic mean ADC was calculated. The thalamus was chosen for internal standardization as it demonstrates less age-related variation compared to white matter structures [10–12]. Also, thalamic ADC values are less dependent on ROI size, show good interobserver agreement and have been used by other authors as internal control [6, 13]. For further corroboration, a statistical analysis of the measured normal thalamic ADC values in this patient population was also performed. The extent of enhancement within each lesion was subjectively categorized as involving 0–25%, 25–50%, 50–75% or 75–100% of the entire lesion. The degree of enhancement was subjectively categorized as mild, moderate and avid.

Statistical Analysis

Descriptive statistics included frequencies and percentages for categorical data, and medians and interquartile ranges (IQR) for continuous variables. Bivariate associations were performed with χ^2 -tests and Fisher's exact tests or Wilcoxon

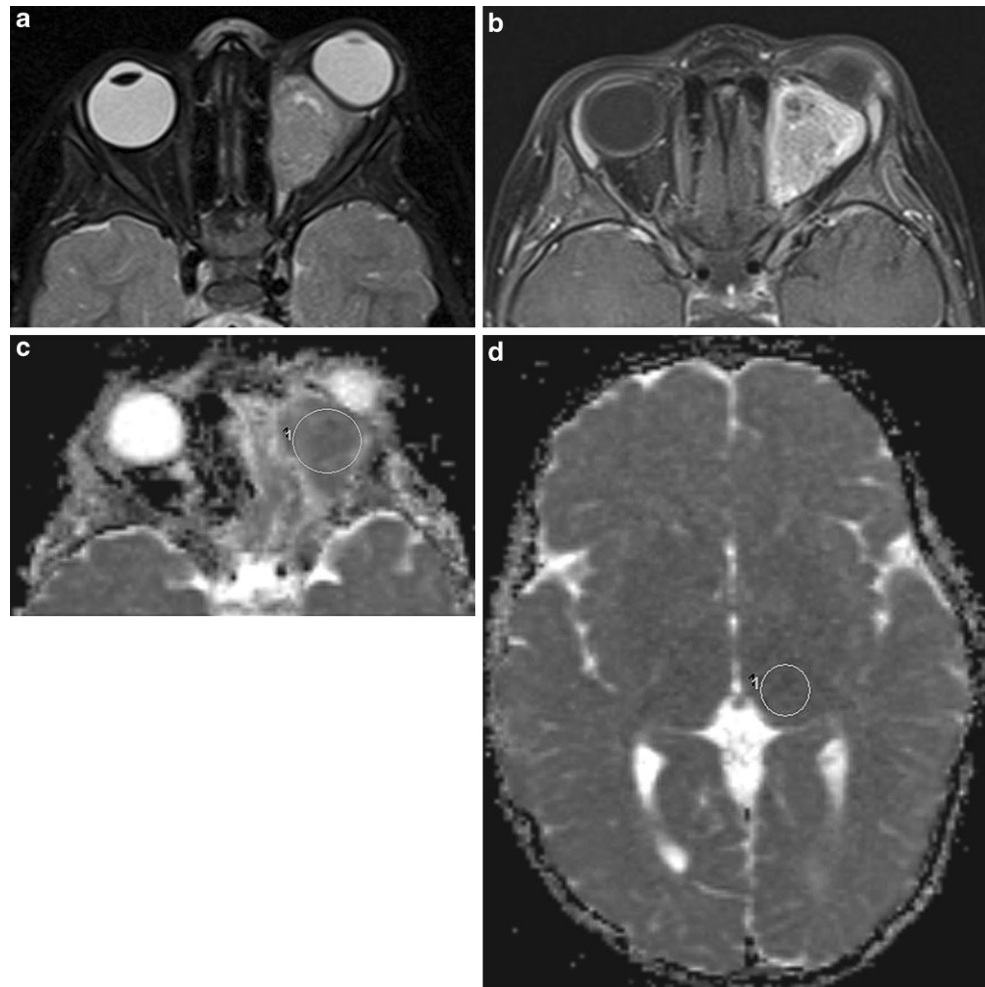
rank sum tests, as appropriate for the data. A receiver operating characteristic (ROC) curve was plotted to provide binary distributions of lesion mean ADC and ADC ratio for malignant lesions. The area under the curve (AUC) was used as a measure of the predictive accuracy. All tests were 2-sided and a *P*-value < 0.05 was considered statistically significant. Data were analyzed using SPSS 24 (IBM Corp, Armonk, NY, USA) and SAS 9.4 (SAS Institute Inc, Cary, NC, USA).

Results

There were a total of 58 patients initially identified, who met the inclusion criteria, 18 patients were excluded because of incomplete image sets, artifacts on DWI images or lesions too small (<5 mm) to adequately be evaluated on the DWI/ADC images. The final analysis included 40 patients, with 31 lesions categorized as benign and 9 as malignant. There were 24 females (60%) and 16 males (40%). The median age was 4.8 years, with a range from 0.6 to 9.2 years. The median age of children with benign lesions was 3.3 years (IQR 0.4–5.9) and for malignant lesions was 9 years (IQR 6.2–9.6). This difference was statistically significant, with *p*-value of 0.01.

The pathological subtypes are detailed in Table 1, and include benign and malignant neoplasms, congenital anomalies, vascular lesions and infectious conditions.

Fig. 2 A 3-year-old male with rapidly progressive proptosis. MRI of the orbits with axial T2 fat-saturated image (a), axial post-contrast T1 fat-saturated image (b), and axial ADC image with ROI placement in the lesion (c). Also shown is axial ADC image with ROI placement in the normal appearing left thalamus (d). There is a mass in the inferior left orbit that has intermediate T2 signal, with small central foci of cystic/necrotic change and heterogeneous post-contrast enhancement. The mass has mean ADC of 0.88 and ADC to thalamic ratio of 1.07, putting it in the malignant category. The mass was determined to be a rhabdomyosarcoma by histopathology



The aggressive lesions included rhabdomyosarcoma ($n=6$) (Figs. 1 and 2), leukemia ($n=2$) and Langerhans cell histiocytosis ($n=1$). There were no cases of lymphoma in this cohort, which is the most common orbital malignancy in adults. The main benign lesions included hemangioma ($n=8$) (Fig. 3) and venolymphatic malformations ($n=10$) (Fig. 4). A substantial subgroup of benign lesions ($n=6$) could not be characterized. These lesions were not biopsied, and the benign nature was deduced from long-term stability by MRI and/or clinical follow-up.

Histopathological confirmation was available in 10 patients. For the rest of the patients, the most likely diagnosis was established taking into account the clinical presentation, past history and the overall imaging appearance on initial and follow-up MRI. For the malignant subgroup, pathological diagnosis was available for all rhabdomyosarcomas and one patient with Langerhans cell histiocytosis (LCH). For two patients with leukemia, the diagnosis was based on blood and bone marrow cytopathology, and response to treatment. For 28 benign lesions without histopathological

diagnosis, the median duration of follow-up was 36 months (IQR 27–48 months).

The median lesion mean ADC for benign lesions was $1.5 \times 10^{-3} \text{ mm}^2/\text{s}$ (IQR 1.2–2 mm^2/s) and for malignant lesions $0.8 \times 10^{-3} \text{ mm}^2/\text{s}$ (IQR 0.7–1 mm^2/s) (Fig. 5). The difference was statistically significant, with a p-value of <0.0001 . The median lesion-to-thalamus ADC ratio for benign lesions was 1.8 (IQR 1.5–2.5) and for malignant lesions 1.1 (IQR 0.9–1.3) (Fig. 6). The difference was statistically significant, with a p-value of <0.001 . The thalamic ADC was within a very narrow range with median of 0.8×10^{-3} (IQR 0.8–0.8) mm^2/s suggesting uniformity across patient ages and technical differences. There were no significant differences in the thalamic ADC between benign and malignant groups.

Receiver operating curve (ROC) analyses were performed for lesion mean ADC value and lesion-to-thalamus ADC ratio (Figs. 7 and 8). For lesion mean ADC, choosing a value that maximizes the sum of the sensitivity and specificity, a cut-off value of $1.14 \times 10^{-3} \text{ mm}^2/\text{s}$ was obtained, giving a sensitivity of 84% and specificity of 100% (Ta-

Fig. 3 A 7-month-old girl with ocular asymmetry. MRI of the orbits with axial (a) and coronal (b) T2 fat-saturated images, axial post-contrast T1 fat-saturated image (c), axial ADC image with ROI placement (d). There is small mass in the lateral extraconal compartment of the left orbit that has intermediate T2 signal, with avid, homogeneous post-contrast enhancement. The mass has facilitated diffusion, with mean ADC of $1.93 \times 10^{-3} \text{ mm}^2/\text{s}$ and ADC to thalamic ratio of 2.31, putting it in the benign category. The mass was presumed to be a capillary hemangioma and followed clinically

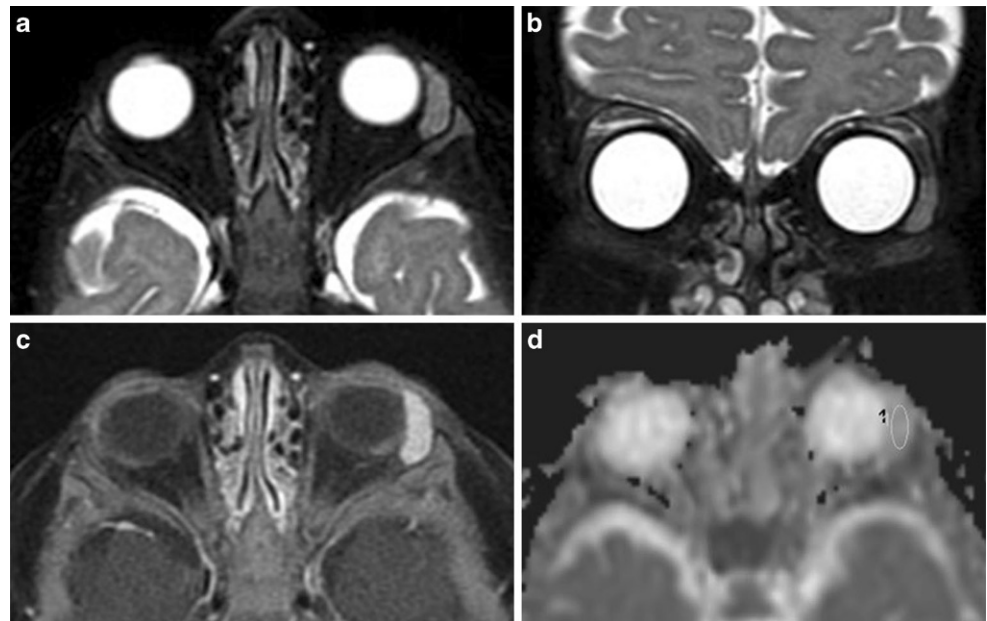
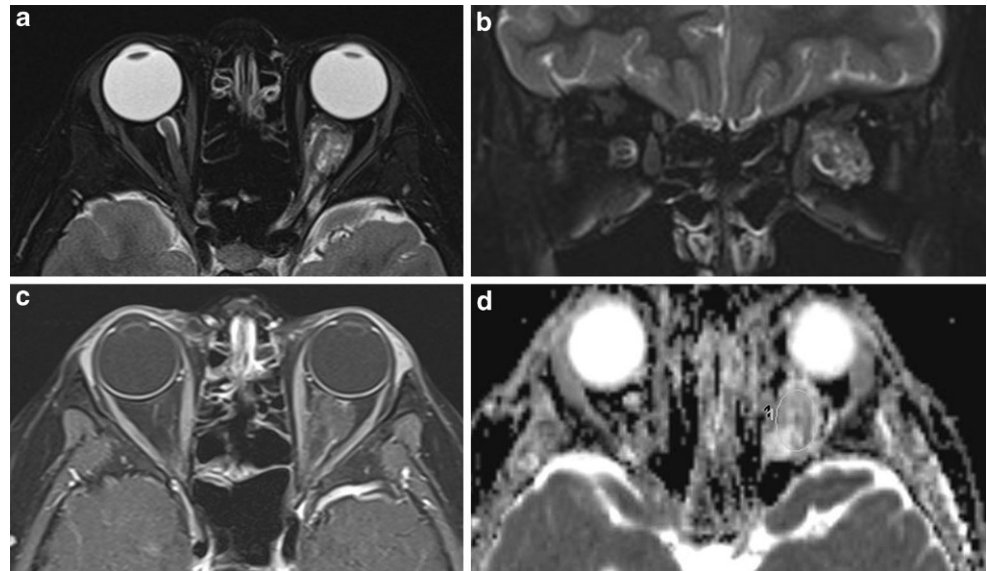


Fig. 4 A 13-year-old boy with proptosis. MRI of the orbits with axial (a) and coronal (b) T2 fat-saturated images, axial post-contrast T1 fat-saturated image (c), axial ADC image with ROI placement (d). There is a heterogeneous mass in the intraconal compartment of the left orbit that has mixed T2 signal and only minimal, patchy post-contrast enhancement. The mass has mean ADC of $1.54 \times 10^{-3} \text{ mm}^2/\text{s}$ and ADC to thalamic ratio of 2.06, putting it in the benign category. This mass was presumed to be a venolymphatic malformation, and decreased in size on multiple follow up studies over the next 3 years



ble 2). For lesion-to-thalamus ADC ratio, a cut-off value of 1.4 was obtained, giving a sensitivity of 81% and specificity of 89% (Table 2).

The lesions were subjectively categorized as bright, intermediate and dark on DWI trace images with 8 lesions being bright, 18 intermediate and 14 dark. Of the DWI bright lesions 4 were benign and 4 malignant, of the DWI intermediate lesions 13 were benign and 5 aggressive and all 14 of the DWI dark lesions were benign. Despite some overlap, there was an overall tendency for malignant lesions to be subjectively brighter on DWI. The lesions were also subjectively categorized as bright, intermediate and dark on T2 and T1-weighted images. On T2-weighted images, 26 lesions were bright, 10 intermediate and 4 dark. There

was no statistically significant association between the lesion type and the subjective T2 signal. On T1-weighted images, 2 lesions were bright, 15 intermediate and 23 were dark, with no statistically significant association.

The presence, extent and degree of enhancement were recorded for each lesion. Malignant lesions had a tendency for greater extent of enhancement, with 8 out of 9 (89%) lesions demonstrating >75% enhancement, compared to 12 out of 31 (39%) of benign lesions demonstrating >75% enhancement. The difference when compared to other subcategories was statistically significant, with $p=0.02$. The degree of enhancement was subjectively categorized as mild, moderate and avid. The differences were not statistically significant. Of the lesions 17 had ill-defined margins,

Fig. 5 Box and whisker plot depicting the distribution of lesion mean ADC for benign and malignant lesions. *Boxes* represent the interquartile range and *whiskers* represent the variability outside the first and third quartiles. The *horizontal line* and the *diamond* (\diamond) represent the median and mean, respectively

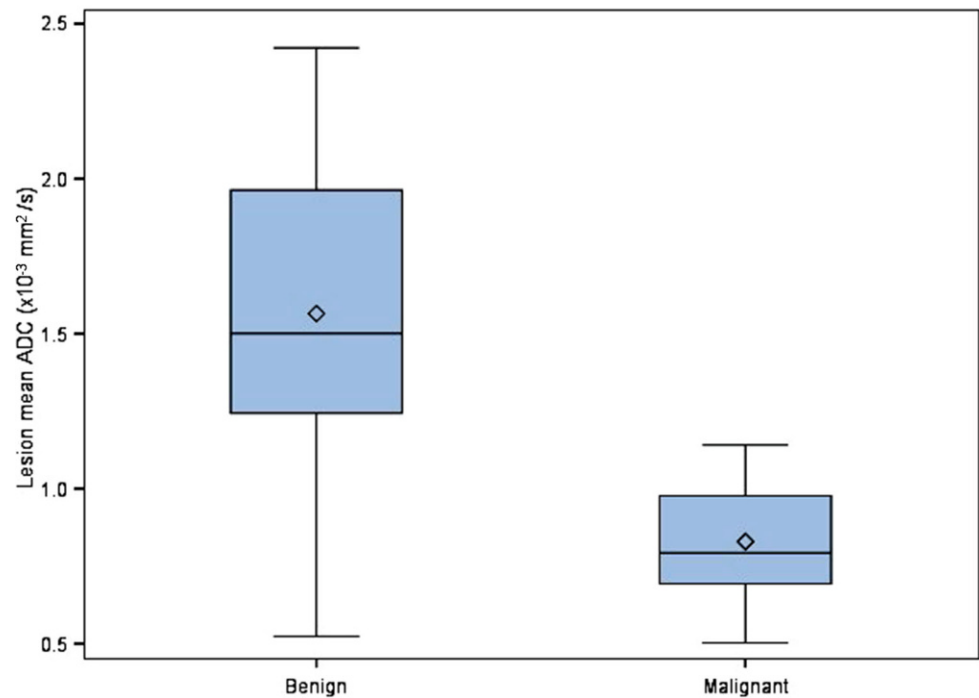
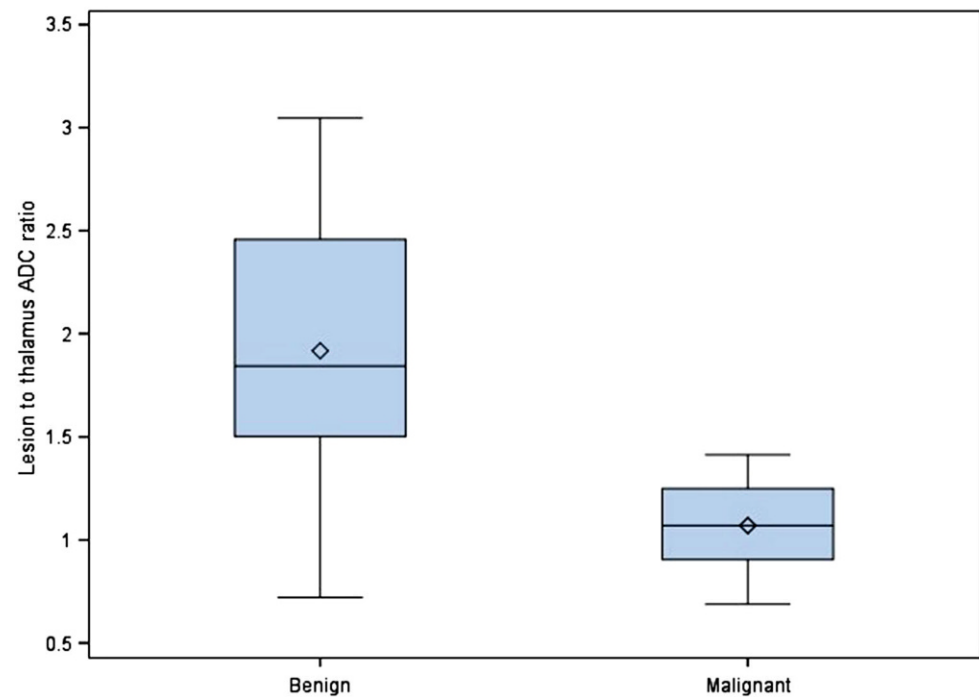


Fig. 6 Box and whisker plot depicting the distribution of lesion-to-thalamus ADC ratio for benign and malignant lesions. *Boxes* represent the interquartile range and *whiskers* represent the variability outside the first and third quartiles. The *horizontal line* and the *diamond* (\diamond) represent the median and mean, respectively

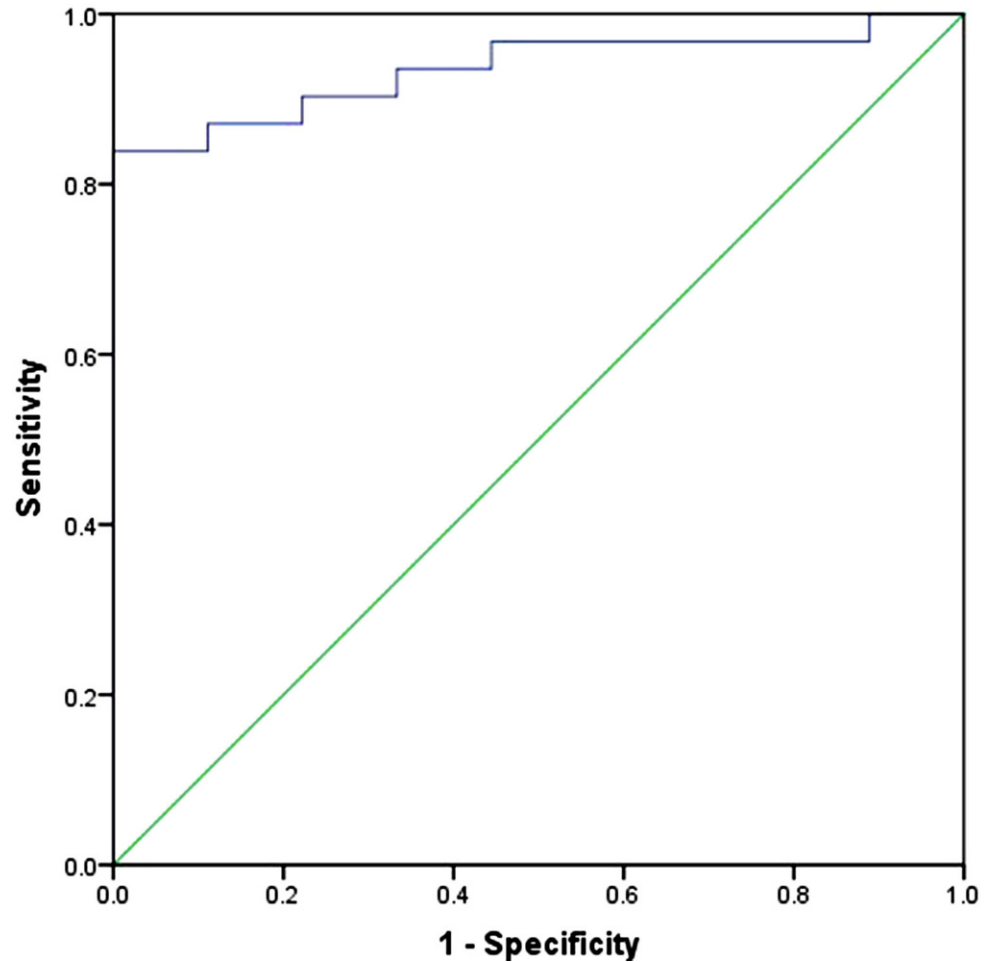


and 23 had well-defined margins, without statistically significant differences between benign and malignant lesion groups. The mean lesion size expressed as a product of three perpendicular dimensions was 7.2cm^3 . There was no statistically significant difference in the lesion sizes between the two groups.

Discussion

A wide spectrum of pediatric orbital pathologies was included in this study, and is fairly representative of what is reported in the literature [1, 14, 15]. The most common pediatric extraocular orbital tumor is rhabdomyosarcoma [1,

Fig. 7 Receiver operating characteristics curve (ROC) for lesion ADC. Area under ROC curve (95% CI) is 0.94 (range 0.86–1). A cut-off value of $1.14 \times 10^{-3} \text{ mm}^2/\text{s}$ gives a sensitivity 84% of and a specificity of 100% in predicting malignant lesions

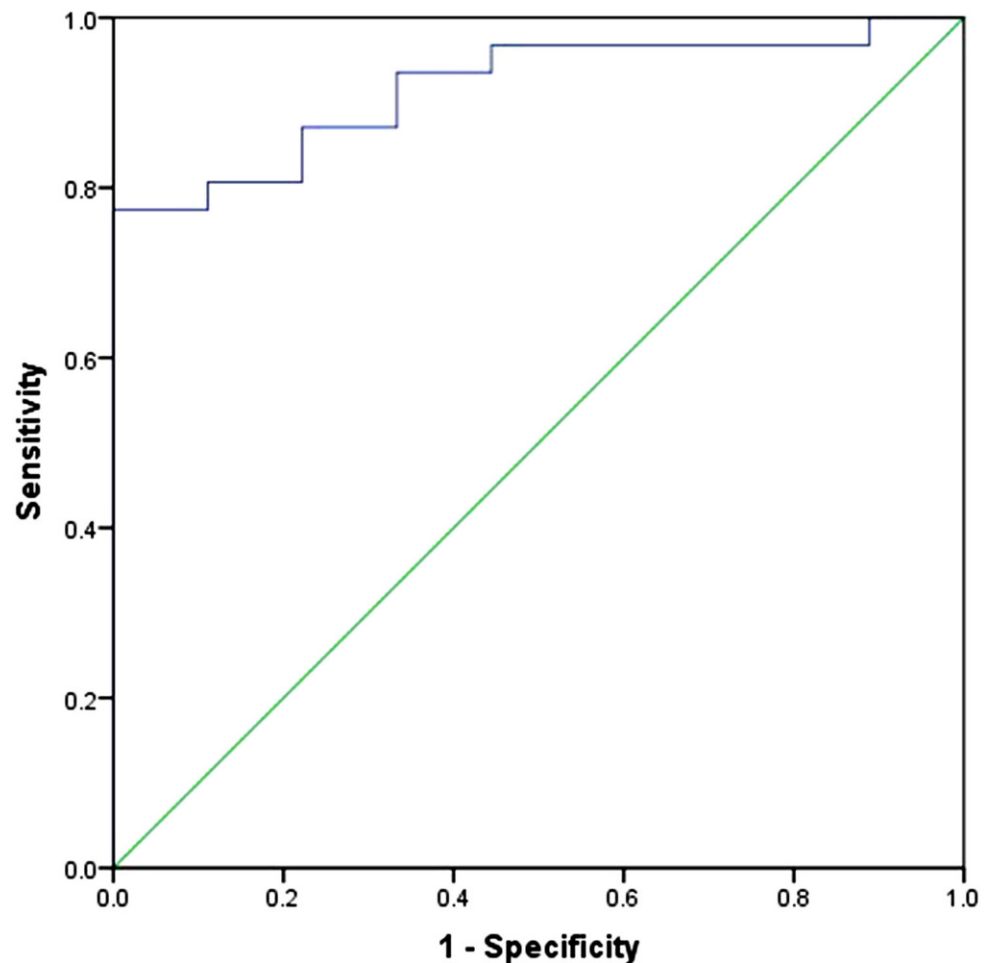


15], which is a highly malignant, rapidly growing lesion. Other common masses are infantile hemangioma, which is a benign vascular neoplasm that involutes on its own, and venolymphatic malformation, which is a developmental vascular anomaly that slowly grows with the patient and can undergo hemorrhage [1, 16]. A number of imaging features were systematically evaluated on orbital MRI. While many features can contribute to narrowing down the differential diagnosis, only diffusion and enhancement characteristics reached statistical significance in distinguishing benign from malignant lesions. The cut-offs for the lesion mean ADC and lesion-to-thalamus ADC ratio that maximized the sensitivity and specificity for prediction of malignant lesions were $1.14 \times 10^{-3} \text{ mm}^2/\text{s}$ and 1.4, respectively. A lower ADC cut-off and lower ADC ratio would improve the specificity at the cost of sensitivity.

Diffusion restriction within a mass has been correlated with increased cellularity and high nuclear to cytoplasmic ratio, which in turn are markers for aggressive neoplasms [17]. The use of quantitative DWI for distinguishing benign from malignant lesions has been most extensively described in the brain [17]; however, it has also been used in

various other body parts including soft tissue lesions of the head and neck [18–20]. The majority of the previously published studies utilizing quantitative DWI for orbital masses focused on adult patients [7–9, 21–23], and covered different pathological entities than are encountered in children. In the few studies that have included pediatric patients, children represent only a minority of the test population, and those results therefore do not adequately reflect the spectrum of pediatric pathologies. For example, the most common malignant lesion in this study was rhabdomyosarcoma, which accounted for only a small proportion of cases in those studies, while lymphoma and metastasis, which represented the majority of malignant lesions in those studies [7–9], were not seen in this population. The majority of benign lesions in this population was of vascular origin and not significantly represented in prior studies. The recently published study by Kralik et al. [24] evaluated the ADC differences between hemangioma and rhabdomyosarcoma in children, which are amongst the commonest pediatric orbital lesions; however, the study did not include the spectrum of pediatric pathology, and especially overlooked the category of clinically and radiologically indeterminate le-

Fig. 8 Receiver operating characteristics curve (ROC) for lesion-to-thalamus ADC ratio. Area under ROC curve (95% CI) is 0.92 (range 0.83–1). A cut-off value of 1.4 gives a sensitivity 81% of and a specificity of 89% in predicting malignant lesions



sions, where a biopsy is not clearly indicated. This group includes vasculogenic lesions and benign tumors of optic nerve, peripheral nerve, meninges and mesenchymal origin. These accounted for 15% of all lesions and 19% of benign lesions in the present study. Their exact incidence is difficult to determine, although these formed a substantial proportion of pediatric orbital masses in prior studies [15, 25]. Lope et al. [26] described the use of DWI in a pediatric population, however, they did not use ADC values and had a smaller sample size.

The proportion of benign and malignant lesions in the present study concurs with a previously published large series that reported 20% of all pediatric orbital masses to be malignant [15]. This study also found a statistically significant difference in the age distribution of benign and malignant masses, with benign lesions seen in younger children. This can be explained by the higher incidence of vasculogenic lesions, such as infantile hemangioma and venolymphatic malformation in infants and younger children, while the peak incidence of rhabdomyosarcoma is 6–8 years [1].

This study has several limitations. This was a retrospective review and the DWI images were obtained across a va-

riety of scanners without standardized techniques. Although ADC values have been found to be reproducible between different scanners and techniques by some reports [21, 27], a recent study has questioned this [28]. The very narrow distribution of mean ADC values of normal appearing thalami in this study argues against the impact of technical differences. Also, lesion-to-thalamus ADC ratios were obtained to mitigate any potential discrepancy arising from this. The sample size is relatively small, which can be attributed to the rarity of these lesions. Moreover, given the variety of pathologies represented, the numbers of individual diagnoses are even smaller. A number of patients had to be excluded, mainly because of lack of DWI images on the studies performed prior to DWI becoming a standard part of orbit MRI protocol in this department, thus introducing a potential source of bias. Histopathological confirmation was available only in a minority of patients, which in part reflects the relatively high risk of biopsy in this region. This also highlights the need for better imaging predictors of malignancy in this population.

This study lends support to the utility of ADC values in assessment of pediatric orbital masses. When other find-

Table 2 Optimal cut-off values for lesion ADC and ADC ratio, with corresponding sensitivity and specificity in distinguishing benign from malignant lesions

	Cut-off	Sensitivity (%)	Specificity (%)
Lesion ADC	1.14 ^a	84	100
ADC ratio	1.4	81	89

ADC apparent diffusion coefficient

^aMean ADC in $\times 10^{-3} \text{ mm}^2/\text{s}$

ings are equivocal, use of ADC values can provide greater confidence in recommending biopsy versus observation or medical treatment. Having an ADC value within the “benign” range can support the decision of watchful waiting in otherwise clinically stable patients. This study provides ADC cut-offs that have reasonable sensitivity and specificity and can be used in conjunction with clinical and conventional imaging findings. Diffusion-weighted images are highly recommended to be a part of any orbital MRI protocol and measuring the ADC value provides an objective method when evaluating intermediate signal on diffusion-weighted images.

In conclusion, ADC values are easily obtained and can be a useful adjunct in MRI evaluation of pediatric orbital masses.

Compliance with ethical guidelines

Conflict of interest A. Jaju, K. Rychlik and M.E. Ryan declare that they have no competing interests.

Ethical standards All procedures performed in the studies involving human participants were in accordance with the ethical standards of the institutional and/or national research committee and with the 1964 Helsinki Declaration and its later amendments or comparable ethical standards. For this retrospective study, the informed consent requirement was waived by the Institutional Review Board. For images or other information within the manuscript which identify patients, consent was obtained from them and/or their legal guardians.

References

- Chung EM, Smirniotopoulos JG, Specht CS, Schroeder JW, Cube R. From the archives of the AFIP: pediatric orbit tumors and tumorlike lesions: nonosseous lesions of the extraocular orbit. *Radiographics*. 2007;27:1777–99.
- Gorospe L, Royo A, Berrocal T, García-Raya P, Moreno P, Abelairas J. Imaging of orbital disorders in pediatric patients. *Eur Radiol*. 2003;13:2012–26.
- Khan SN, Sepahdari AR. Orbital masses: CT and MRI of common vascular lesions, benign tumors, and malignancies. *Saudi J Ophthalmol*. 2012;26:373–83.
- Burns NS, Iyer RS, Robinson AJ, Chapman T. Diagnostic imaging of fetal and pediatric 12 orbital abnormalities. *AJR Am J Roentgenol*. 2013;201:W797–808.
- Rao AA, Naheedy JH, Chen JY, Robbins SL, Ramkumar HL. A clinical update and radiologic review of pediatric orbital and ocular tumors. *J Oncol*. 2013;2013:975908.
- Sepahdari AR, Kapur R, Aakalu VK, Villablanca JP, Mafee MF. Diffusion-weighted imaging of malignant ocular masses: initial results and directions for further study. *AJNR Am J Neuroradiol*. 2012;33:314–9.
- Sepahdari AR, Aakalu VK, Setabutr P, Shiehorteza M, Naheedy JH, Mafee MF. Indeterminate orbital masses: restricted diffusion at MR imaging with echo-planar diffusion-weighted imaging predicts malignancy. *Radiology*. 2010;256:554–64.
- Razek AA, Elkhamary S, Mousa A. Differentiation between benign and malignant orbital tumors at 3-T diffusion MR-imaging. *Neuroradiology*. 2011;53:517–22.
- Fatima Z, Ichikawa T, Ishigame K, Motosugi U, Waqar AB, Hori M, Iijima H, Araki T. Orbital masses: the usefulness of diffusion-weighted imaging in lesion categorization. *Clin Neuroradiol*. 2014;24:129–34.
- Morriss MC, Zimmerman RA, Bilaniuk LT, Hunter JV, Haselgrove JC. Changes in brain water diffusion during childhood. *Neuroradiology*. 1999;41:929–34.
- Mukherjee P, Miller JH, Shimony JS, Conturo TE, Lee BC, Almi CR, McKinstry RC. Normal brain maturation during childhood: developmental trends characterized with diffusion-tensor MR imaging. *Radiology*. 2001;221:349–58.
- Forbes KP, Pipe JG, Bird CR. Changes in brain water diffusion during the 1st year of life. *Radiology*. 2002;222:405–9.
- Bilgili Y, Unal B. Effect of region of interest on interobserver variance in apparent diffusion coefficient measures. *AJNR Am J Neuroradiol*. 2004;25:108–11.
- Viswanathan S, George S, Ramadwar M, Shet T, Arora B, Laskar S, Qureshi S, Medhi S, Muckaden MA, Kurkure PA, Kane SV, Banavali S. Extraconal orbital tumors in children—a spectrum. *Virchows Arch*. 2009;454:703–13.
- Shields JA, Shields CL, Scartozzi R. Survey of 1264 patients with orbital tumors and simulating lesions: The 2002 Montgomery Lecture, part 1. *Ophthalmology*. 2004;111:997–1008.
- Smoker WR, Gentry LR, Yee NK, Reede DL, Nerad JA. Vascular lesions of the orbit: more than meets the eye. *Radiographics*. 2008;28:185–204.
- Cha S. Update on brain tumor imaging: from anatomy to physiology. *AJNR Am J Neuroradiol*. 2006;27:475–87.
- Koontz NA, Wiggins RH 3rd. Differentiation of benign and malignant head and neck lesions with diffusion tensor imaging and DWI. *AJR Am J Roentgenol*. 2017;208:1110–5.
- Wang J, Takashima S, Takayama F, Kawakami S, Saito A, Matsushita T, Momose M, Ishiyama T. Head and neck lesions: characterization with diffusion-weighted echo-planar MR imaging. *Radiology*. 2001;220:621–30.
- Srinivasan A, Mohan S, Mukherji S. Biologic imaging of head and neck cancer: the present and the future. *AJNR Am J Neuroradiol*. 2012;33:586–94.
- Sepahdari AR, Politi LS, Aakalu VK, Kim HJ, Razek AA. Diffusion-weighted imaging of orbital masses: multi-institutional data support a 2-ADC threshold model to categorize lesions as benign, malignant, or indeterminate. *AJNR Am J Neuroradiol*. 2014;35:170–5.
- Politi LS, Forghani R, Godi C, Resti AG, Ponzoni M, Bianchi S, Iadanza A, Ambrosi A, Falini A, Ferreri AJ, Curtin HD, Scotti G. Ocular adnexal lymphoma: diffusion-weighted MR imaging for differential diagnosis and therapeutic monitoring. *Radiology*. 2010;256:565–74.
- EiKhamary SM, Galindo-Ferreiro A, AlGhafri L, Khandekar R, Schellini SA. Characterization of diffuse orbital mass using Apparent diffusion coefficient in 3-tesla MRI. *Eur J Radiol Open*. 2018;5:52–57.
- Kralik SF, Haider KM, Lobo RR, Supakul N, Calloni SF, Soares BP. Orbital infantile hemangioma and rhabdomyosarcoma in chil-

- dren: differentiation using diffusion-weighted magnetic resonance imaging. *J AAPOS*. 2018;22:27–31.
25. Kodsi SR, Shetlar DJ, Campbell RJ, Garrity JA, Bartley GB. A review of 340 orbital tumors in children during a 60-year period. *Am J Ophthalmol*. 1994;117:177–82.
 26. Lope LA, Hutcheson KA, Khademian ZP. Magnetic resonance imaging in the analysis of pediatric orbital tumors: utility of diffusion-weighted imaging. *J AAPOS*. 2010;14:257–62.
 27. Chenevert TL, Galbán CJ, Ivancevic MK, Rohrer SE, Londy FJ, Kwee TC, Meyer CR, Johnson TD, Rehemtulla A, Ross BD. Diffusion coefficient measurement using a temperature-controlled fluid for quality control in multicenter studies. *J Magn Reson Imaging*. 2011;34:983–7.
 28. Kıvrak AS, Paksoy Y, Erol C, Koplay M, Özbek S, Kara F. Comparison of apparent diffusion coefficient values among different MRI platforms: a multicenter phantom study. *Diagn Interv Radiol*. 2012;19:433–7.